High efficiency dye-sensitized solar cells exploiting sponge-like ZnO nanostructures

# PCCP

## Accepted Manuscript



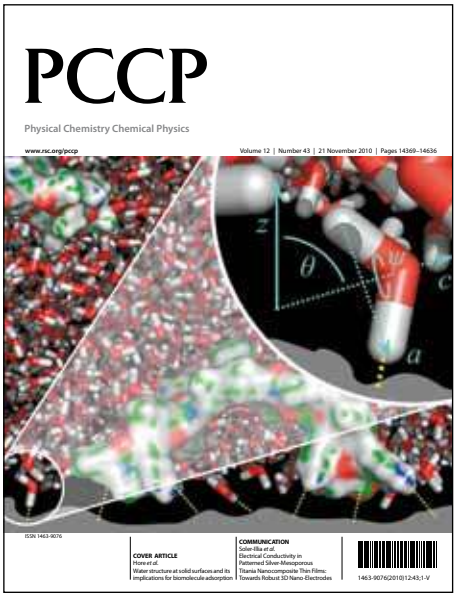


This is an *Accepted Manuscript*, which has been through the RSC Publishing peer review process and has been accepted for publication.

*Accepted Manuscripts* are published online shortly after acceptance, which is prior to technical editing, formatting and proof reading. This free service from RSC Publishing allows authors to make their results available to the community, in citable form, before publication of the edited article. This *Accepted Manuscript* will be replaced by the edited and formatted *Advance Article* as soon as this is available.

To cite this manuscript please use its permanent Digital Object Identifier (DOI®), which is identical for all formats of publication.

More information about *Accepted Manuscripts* can be found in the **Information for Authors**.

Please note that technical editing may introduce minor changes to the text and/or graphics contained in the manuscript submitted by the author(s) which may alter content, and that the standard **Terms & Conditions** and the **ethical guidelines** that apply to the journal are still applicable. In no event shall the RSC be held responsible for any errors or omissions in these *Accepted Manuscript* manuscripts or any consequences arising from the use of any information contained in them.

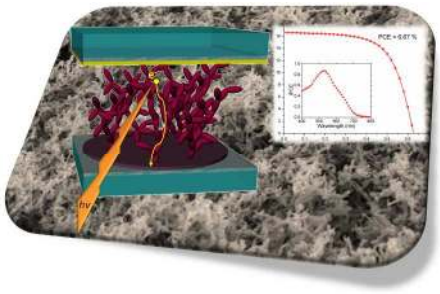

DSCs based on sponge-like ZnO photoanodes showing conversion efficiency of 6.67% and superior transport properties compared with standard $TiO_2$ nanoparticles.

View Online

Cite this: DOI: 10.1039/c0xx00000x

www.rsc.org/pccp

PAPER

# High efficiency Dye-sensitized Solar Cell exploiting sponge-like ZnO nanostructures

**Adriano Sacco,*[a] Andrea Lamberti,[a,b] Rossana Gazia,[a] Stefano Bianco,[a] Diego Manfredi,[a] Nadia Shahzad,[a,b] Federica Cappelluti,[c] Shuai Ma,[c] and Elena Tresso[a,b]**

*Received (in XXX, XXX) Xth XXXXXXXXX 20XX, Accepted Xth XXXXXXXXX 20XX*

**DOI: 10.1039/b000000x**

Sponge-like nanostructured ZnO layers were successfully employed as photoanodes for the fabrication of highly efficient DSCs. The sponge-like ZnO layers were obtained by room temperature radio-frequency magnetron sputtering deposition of metallic zinc, followed by thermal oxidation treatment in ambient atmosphere. The porous films show a 3D branched nanomorphology, with a feature similar to natural coral. The morphological and optical properties of these layers were studied through field emission scanning electron microscopy, specific surface area measurements, ultraviolet-visible transmittance and absorption spectroscopy. The sponge-like ZnO film presents a high density of branches, with a relatively high specific area value, and fine optical transmittance. The morphology of the porous structure provides a high number of adsorption sites for the anchoring of sensitizer molecules, making it suitable for the fabrication of ZnO-based photoanode for Dye-sensitized Solar Cells. The light harvesting performance of the sensitized semiconductor was evaluated by current density vs. voltage measurements, incident photon-to-electron conversion efficiency, open circuit voltage decay and impedance spectroscopy. The modelling of the electrical characteristics evidences a higher electron lifetime and a longer charge diffusion length, if compared to standard $TiO_2$ nanoparticle based photoanodes. For ZnO films with a thickness up to 18 µm, a photoconversion efficiency as high as 6.67% and a maximum value of the incident photon-to-electron collection efficiency equal to 87% at 530 nm were demonstrated.





## 1. Introduction

Nowadays the continuously boosting energy demand and the overall increase in energy consumption have driven huge interest towards new types of energy supply. Currently fossil fuels lead the energy market, but their increasing cost, the finite supply of their sources and the long-term effects of $CO_2$ emission are making the research for renewable energy sources, like photovoltaics (PV), more and more urgent and necessary. PV market is currently dominated by silicon technology, which provides high photoconversion efficiency for terrestrial applications, but is not always cost effective, due to the use of expensive raw materials and highly energy consuming process technologies. Conversely, Dye-sensitized Solar Cells (DSCs) represent one of the most interesting non-silicon solar harvesters, with outstanding potential as low-cost devices, suitable for large area production, and characterized by the ease of their fabrication process. First proposed more than twenty years ago[1], these photoelectrochemical cells are constituted by a dye-sensitized photoanode, a hole-conducting material and a counter electrode. The photoanode consists of a glass slide covered with a Transparent Conducting Oxide (TCO) film, on which a layer of a porous wide bandgap semiconductor is deposited. The semiconductor surface is sensitized with dye molecules, which absorb the light and generate electrons that, passing through the oxide layer, are collected by the front electrode. A redox couple acts as hole conductor, electrically regenerating the dye molecules. The counter electrode is a TCO-covered glass slide with a thin Pt layer that catalyzes the redox reaction. At present, the highest photovoltaic conversion efficiency, exceeding 12%, has been obtained using titanium dioxide nanoparticles as photoanode material, porphyrin molecules as sensitizer and cobalt (II/III) as redox shuttle[2].

Zinc oxide is a promising material alternative to $TiO_2$ for the fabrication of DSC photoanodes. It presents some resemblances with $TiO_2$, such as a similar band gap and a conduction band edge located almost at the same level, and some advantages, like higher electron mobility and lifetime[3]. A great number of one-dimensional ZnO nanostructures, like nanowires or nanorods[4,5], can be easily grown, as well as more complex three-dimensional structures such as branched and dendritic nanowires[6-9]. The 1D structures are characterized by superior charge transport properties along the *c*-axis direction but, if compared to nanoparticles, they exhibit a reduced value of exposed area. A high specific surface is a crucial feature in a DSC photoanode, since it determines the maximum number of anchored dye molecules. The resulting photovoltaic performances of low-dimensional nanostructured ZnO electrodes are therefore rather poor[10]. On the other hand, 3D branched/dendritic structures can

show good transport properties, at the same time maintaining a discrete number of sites for dye sensitization. However, the higher degree of complexity limits the reproducibility of the fabrication process and the scalability towards larger area devices[10]. At present, the photoconversion efficiencies of ZnO-based DSCs using Ru-based sensitizer and $I^-/I_3^-$ redox couple are below 8%[10-12], so the development of new structures and/or architectures able to improve the cell performances is an exciting challenge.

We recently proposed a method for the production of ZnO photoanodes[13,14], which is very easy, low cost and scalable for large area device fabrication. The method consists in the deposition of a sponge-like Zn layer onto TCO-covered glass substrates by radio-frequency (RF) magnetron sputtering technique at room temperature, followed by a thermal oxidation of the Zn film in ambient atmosphere. The obtained nanoporous ZnO films show a pure wurtzite crystalline structure and a branched morphology. ZnO-based DSCs with remarkable efficiency were successfully fabricated with a microfluidic architecture[15].

In the present work, we focus on the optical and transport properties of this sponge-like material. We examine ZnO films with thicknesses up to 18 µm. They exhibit a high-density of branches, with a relatively high specific area, a good dye loading, and a high transparency to the visible light, that make them suitable for applications in solar windows. Furthermore, by means of a deeper analysis on the charge carrier lifetime and the evaluation of the electron diffusion length, we evidence the faster transport in sponge-like ZnO with respect to mesoporous $TiO_2$. Finally we demonstrate that using ZnO films with a thickness of 18 µm in an irreversibly sealed architecture a photoconversion efficiency value as high as 6.67% can be reached.

## 2. Experimental

### 2.1 Materials and device fabrication

A detailed description of the fabrication of ZnO-based photoanode was reported elsewhere[13,14]. Briefly, the photoanodes were prepared by depositing onto Fluorine-doped Tin Oxide (FTO) coated glass sponge-like zinc films by RF magnetron sputtering at room temperature, using argon as sputtering gas. In this work, the thickness of nanostructured Zn layers was increased up to 18 µm. A thermal treatment carried out in ambient air on a hot plate at 380 °C was employed for oxidizing the zinc films in order to obtain sponge-like ZnO layers. After the fabrication, the photoanodes were heated at 70 °C, soaked at room temperature into a 0.25 mM N719 ethanol-based dye solution (Ruthenizer535bis-TBA, Solaronix) and then rinsed in pure ethanol to remove the un-adsorbed molecules. According to our previous study[14], 2 h was chosen as incubation time. In order to compare the properties of the sponge-like ZnO with the most commonly used material in DSCs, $TiO_2$ nanoparticle-based photoanodes were also prepared, using our standard previously reported procedure[16], with an 8 µm-thick $TiO_2$ film obtained by a commercial paste (Ti-Nanoxide D37, Solaronix.

The counter electrodes were firstly drilled in order to create the inlet port for electrolyte filling, then cleaned and coated with a 5 nm thick Pt thin film using the procedure described elsewhere[15]. The two electrodes were subsequently sealed together employing a 25 µm thick thermoplastic spacer (Meltonix 1170-25/PF, Solaronix) heated in a hot press at 90 °C applying a slight pressure. The cells were then filled with the electrolyte (Iodolyte AN50, Solaronix) using a vacuum procedure and the inlet hole was sealed by using a glass slice and the thermoplastic film as bonding material.

### 2.2 Characterization

The morphology of the ZnO nanostructures was investigated by means of a Zeiss Supra 40 Field Emission Scanning Electron Microscope (FESEM), both in top view and in cross view (with electron energy of 5 keV). Brunauer–Emmett–Teller (BET) specific surface area was measured from $N_2$ sorption isotherms (Quantachrome Autosorb1) by multipoint method within the relative pressure range of 0.1–0.3 $P/P_0$.

UV-visible spectroscopy measurements (in transmittance and absorbance) were carried out using a Varian Cary 5000 spectrophotometer. The amount of dye loading on the photoanode was determined by desorbing the dye molecules from the oxide using a known volume of 0.1 M NaOH aqueous solution, measuring the optical absorbance. The concentration of this ensuing solution and hence the total number of adsorbed dye molecules were calculated employing the Lambert-Beer law and the pre-determined extinction coefficient value (12717 $M^{-1}$ $cm^{-1}$ at 500 nm) of dye in the corresponding basic solution[17].

I-V electrical characterizations under AM1.5G illumination (100 $mW/cm^2$) were performed using a class A solar simulator (Newport 91195A) and a source measure unit (Keithley 2440). Incident Photon-to-electron Collection Efficiency (IPCE) measurements were carried out using a 100 W QTH lamp (Newport) as light source, a 150 mm Czerny Turner monochromator (Lot-Oriel Omni-λ 150) and a source measure unit (Keithley 2440) for collecting the DC current. Open Circuit Voltage Decay (OCVD) curves were acquired using an electrochemical workstation (CH Instruments 760D) with a time resolution of 100 ms. Electrochemical impedance spectra (EIS) were collected in dark condition through an electrochemical workstation (CH Instruments 760D) in the frequency range between 100 mHz and 20 kHz, at different applied bias voltage, with an amplitude of the sinusoidal signal of 10 mV.

## 3. Results and discussion

The growth mechanisms, the composition and the crystallographic phase of the sponge-like ZnO films were previously investigated[13,14], revealing the formation of stoichiometric ZnO layers with a hexagonal wurzitic structure. In Fig. 1a the cross-sectional FESEM micrograph of the investigated ZnO film is reported. The film exhibits a compact morphology within few tens of nm from the interface with FTO, which is formed during the first stages of the deposition. This thin denser layer spontaneously evolves into a more branched structure, due to the increase of substrate temperature caused by the interaction between plasma and substrate surface.[13] The resulting sponge-like film had a maximum thickness of about 18 µm. The inset of Fig. 1a shows a higher magnification 45°-tilted view in which it is possible to appreciate the sponge-like nature of the nanostructured ZnO layer, with a feature similar to natural coral.

The cartoon in Fig. 1b schematically represents the front-side illuminating configuration in which the sponge-like ZnO Dye-sensitized Solar Cells were assembled and characterized.

The shape and position of the hysteresis loops of the nitrogen sorption isotherm reported in Fig. 2 are compatible with the branched porous ZnO structure. The calculated specific area of the material is 14.1 $m^2/g$. This value is lower than in nanoparticulated $TiO_2$ electrodes usually employed in DSCs, but comparable to that of other ZnO layers reported in literature[9,18].

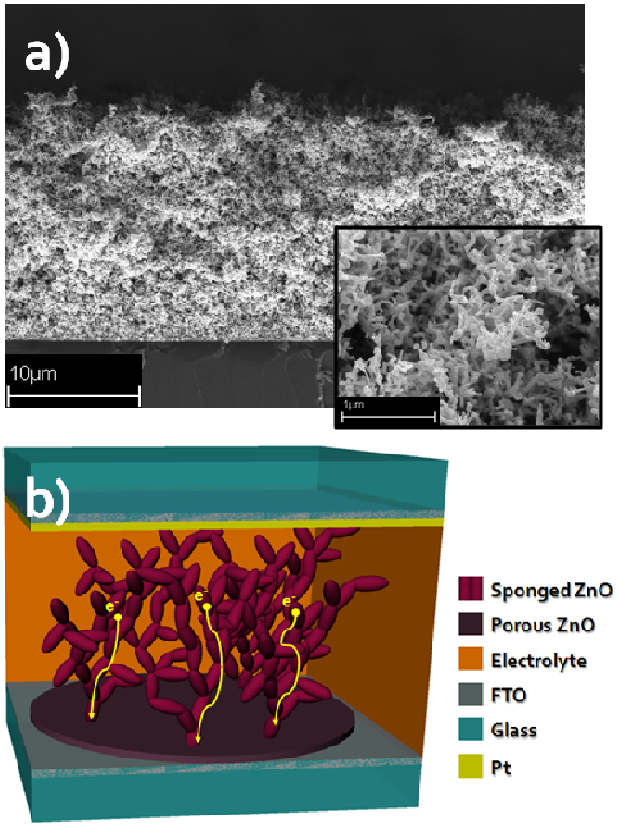


**Fig. 1** (a) FESEM micrographs showing the ZnO cross-sectional view and a higher magnified view of the tilted top of the sponge-like layer (reported in the inset). (b) Architecture of a DSC employing the ZnO porous layer as photoanode.

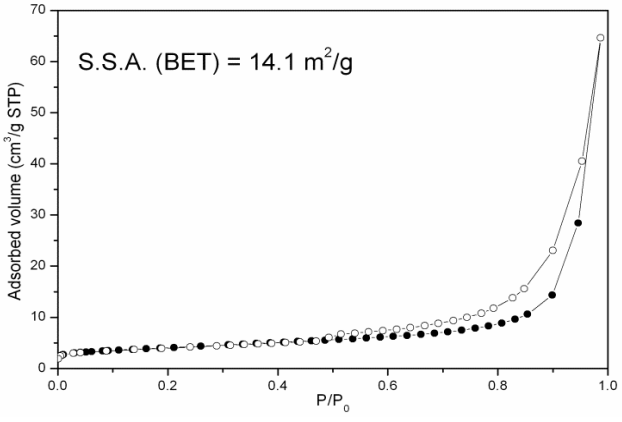


**Fig. 2** $N_2$ sorption isotherms for the surface area evaluation.

The UV-visible direct transmittance of sponge-like ZnO and nanoparticulated $TiO_2$ films with the same thickness (8 μm) deposited on the same kind of transparent conductive substrates were measured and compared, and the obtained optical spectra are reported in Fig. 3. The effect of the thermal oxidation on the

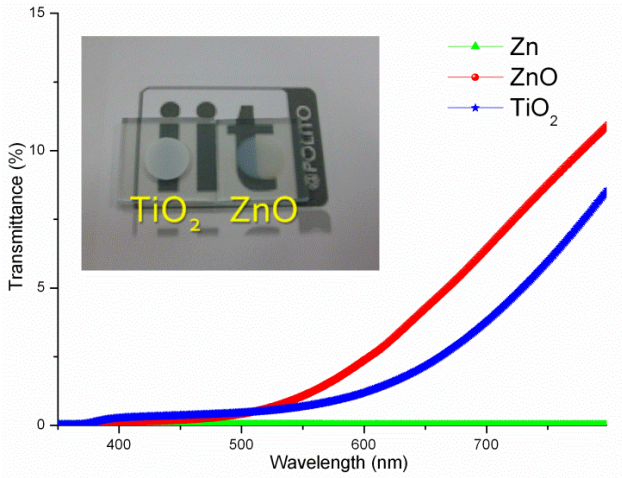


**Fig. 3** UV-visible transmittance curves obtained for the Zn, ZnO and $TiO_2$ layers on transparent conductive substrates with the same thickness (8 μm). The two metal-oxide photoanodes are visualized in the inset.

Zn film is evident: the transmittance was approximately zero for the metallic film, while a semi-transparent layer was obtained after the oxidation. It is well known that thin $TiO_2$ films made with small (8-10 nm) anatase particles can give high transmittance, but it has to be observed that such films do not contain the larger (>100 nm) optically dispersing titania particles which permit to obtain high light conversion efficiencies. For this reason the ZnO transmittance spectrum has been compared to the one obtained on a $TiO_2$ film made with an opaque and dispersing $TiO_2$ paste and in this case the ZnO transmittance is definitely higher, as can be observed in Fig. 3. This result is promising for the possibility of employing sponge-like ZnO in transparent DSCs for solar windows applications.

Moreover, by means of a washing procedure, the dye loading value was found to be 6.2 x $10^{-8}$ moles/$cm^2$. This value shows that, despite the lower specific surface area, the dye loading on sponge-like ZnO photoanode is comparable to what reported in literature for $TiO_2$ nanoparticulated films (ranging from 5 x $10^{-8}$ to 14 x $10^{-8}$ moles/$cm^2$ with thicknesses lying in the range of 12 – 15 μm)[19-20].

In Fig. 4, the results of the photovoltaic characterization under AM1.5G illumination are reported. The cells fabricated with 18 μm thick ZnO photoanodes immersed for 2 h in N719 solution exhibit a short circuit current density ($J_{SC}$) of 16.63 mA/$cm^2$, an open circuit voltage ($V_{OC}$) of 628 mV and a Fill Factor (*FF*) of 0.64, leading to the noticeable PhotoConversion Efficiency (*PCE*) value of 6.67%. The 2 h impregnation time is optimal to avoid the formation of aggregates between N719 dye molecules and dissolved $Zn^{2+}$ ions coming from the ZnO surface. This effect is well known for ZnO in presence of metal-organic dyes and could bring to a decrease of the efficiency for long incubation time[14,21]. The inset of Fig. 4 shows the Incident Photon-to-electron Collection Efficiency spectrum: the IPCE curve is above 0.5 in the wavelength range from 400 to 600 nm, with a maximum value of 0.87 measured at 530 nm.

Such promising results can be explained by the reduced charge

recombination kinetic in the ZnO-based cells. For this reason we performed open circuit voltage decay measurements and the results were compared to standard $TiO_2$ nanoparticle-based

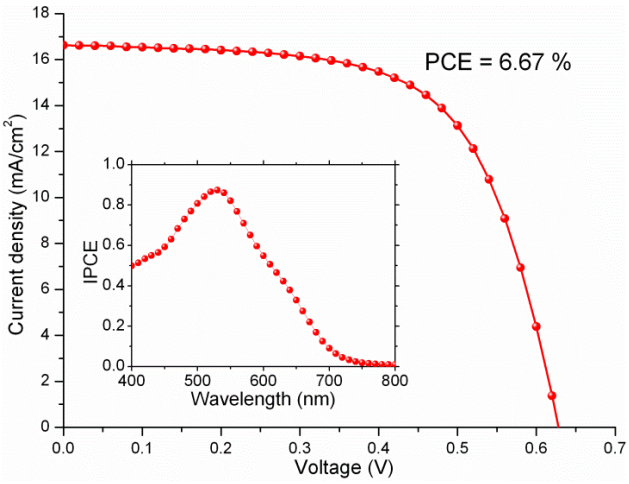


**Fig. 4** Current density-voltage curve of 18 µm thick ZnO-based DSC. In the inset, the relative IPCE spectrum is shown.

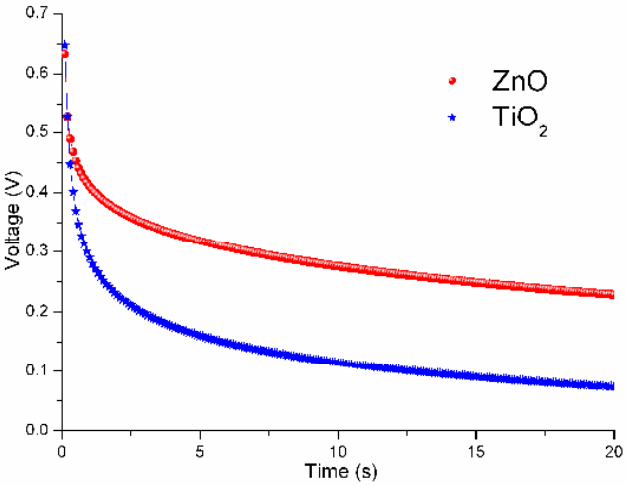


**Fig. 5** Open circuit voltage decay curves of 18 µm thick ZnO-based and 8 µm thick $TiO_2$-based DSCs.

DSCs. The $V_{OC}$ was recorded during relaxation from an illuminated quasi-equilibrium state to the dark equilibrium. When the illumination of the DSC at open circuit condition is interrupted, the excess electrons recombine, so the photovoltage decay rate is related to electron lifetime[22]. The results of the OCVD measurements performed on the cells are reported in Fig. 5. A slower decay of the open circuit voltage (evidencing a superior charge lifetime) was observed for the ZnO-based cells: the morphological properties of the sponge-like structure may contribute reducing the number of defects and trap sites, thus lowering the recombination rate with respect to the nanoparticle-based photoanode[23].

Electrochemical impedance spectroscopy analysis allowed to confirm the above results and to study the transport properties of the ZnO nanostructures. The experimental EIS data were fitted using the equivalent circuit shown in Fig. 6, which includes contact resistance ($R_S$), equivalent impedance of the photoanode ($Z_{ox}$), and a charge transfer impedance ($R_{CE}$ and $C_{CE}$) at the electrolyte-cathode interface[24]. The mass transport impedance due to the diffusion of electrolyte species has been neglected since no significant contribution was evidenced in the measured frequency range. According to a purely diffusive transport model of electrons across the photoanode, the small-signal impedance of the oxide is modelled by the input impedance of the distributed RC circuit, open load terminated, shown in Fig. 6 (bottom)[25].

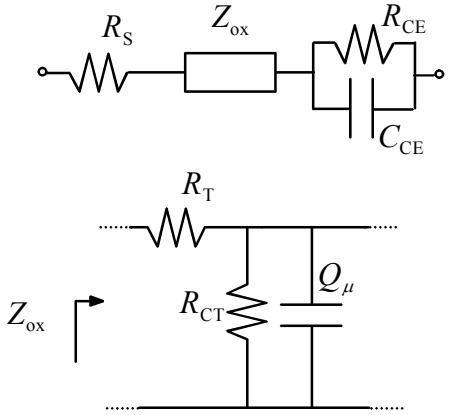


**Fig. 6** Equivalent circuit exploited for the fitting of the EIS spectra. Top: equivalent circuit of the overall cell. Bottom: transmission line model of the oxide film.

The constant phase element $Q_\mu$ with equivalent impedance

$$Z = Q_\mu^{-1}(i\omega)^{-\beta} \quad (1)$$

is a generalization of the conventional electrochemical capacitance, included to account for the possible frequency dispersion observed in the EIS spectra. The electrochemical capacitance $C_\mu$, corresponding to the constant phase element results as

$$C_\mu = Q_\mu^{\frac{1}{\beta}} R_{CT}^{\frac{1}{\beta}-1} \quad (2)$$

A few examples of Nyquist plots comparing the measured EIS spectra with the calculated ones are shown in Fig. 7. Measured and fitted EIS spectra at open circuit voltage of the ZnO based and $TiO_2$-based DSCs are compared in Fig. 7a. The high frequency semicircles are ascribed to the impedance of the $R_{CE}$, $C_{CE}$ parallel, while the larger semicircles in the low frequency range are associated to the recombination mechanisms in the oxide film ($R_{CT}$, $Q_\mu$). Here $R_T$ is nearly invisible, since it overlaps with the counter electrode impedance arc. The contribution of $R_T$ and its bias dependence are shown in Fig. 7b for the ZnO-based cell. From the fitting parameters $R_T$, $R_{CT}$, $Q_\mu$ and $\beta$, the effective electron lifetime $\tau_n$, the diffusion length $L_n$ and the diffusion coefficient $D_n$ were evaluated according to the following equations:

$$\tau_n = (R_{CT} Q_\mu)^{1/\beta} \quad (3)$$

$$L_n = d\sqrt{R_{CT}/R_T} \quad (4)$$

$$D_n = L_n^2 / \tau_n \quad (5)$$

where *d* is the thickness of the oxide layer.

With the aim to compare the transport properties of the two different oxides, it is convenient to use as reference quantity the electrochemical capacitance instead of the applied voltage. In fact, within the framework of a multiple-trapping model, and assuming an exponential trap density of states, $C_\mu$ turns to be approximately proportional to the electron density within the

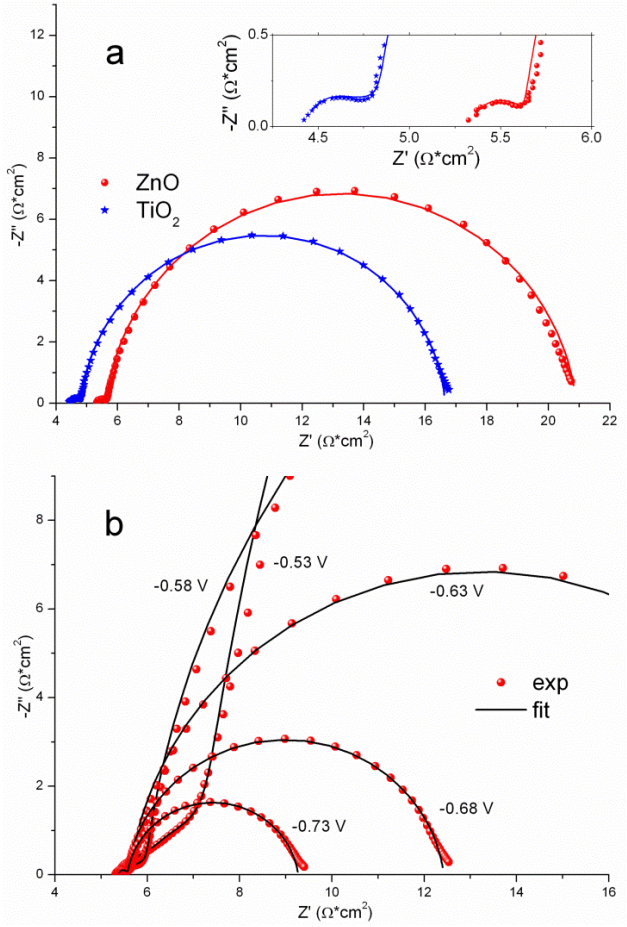


**Fig. 7** (a) Measured (symbols) and fitted (solid line) EIS spectra at open circuit voltage of 18 µm thick ZnO-based and 8 µm thick $TiO_2$-based DSCs. The high frequency zoom is reported in the inset. (b) High frequency behaviour of the ZnO based cell impedance: measurements (symbols) and fitting (solid lines) at applied voltage ranging from -0.53 V to -0.73 V with 0.05 V step.

oxide[26,27]. Fig. 8 reports the dependence of the effective lifetime and the diffusion coefficient as a function of the electrochemical capacitance $C_\mu$ as obtained from the EIS analysis. As expected from OCVD results, the electron lifetime values for the sponge-like ZnO are higher than those reported for $TiO_2$ nanoparticle, thus evidencing the lower recombination rate (probably due to a reduced number of surface defects of the three-dimensional structure). Moreover, the sponge-like layer can improve the electron transport through the dye-sensitized photoanode by exploiting a pathway for photogenerated electron collection that is less tortuous than that of randomly interconnected nanoparticles[10]. As a consequence, the ZnO-based DSCs are characterized by increased diffusion coefficient values. Using equation (4), the diffusion length values of the two cells, at open circuit voltage, were found to be about 100 µm and 30 µm for the sponge-like based cell and the $TiO_2$ nanoparticle-based cell, respectively. The measured diffusion length for the coral-shaped ZnO is approximately one order of magnitude lower than that measured for 1D ZnO nanowires[28,29] and two orders of magnitude higher with respect to isotropic ZnO nanoparticles[30]. These results confirm the enhanced transport properties of the proposed ZnO layer.

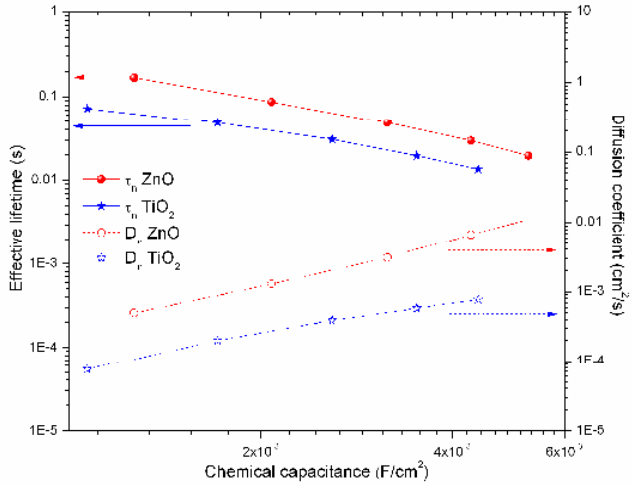


**Fig. 8** Effective electron lifetime and diffusion coefficient dependence on the chemical capacitance for 18 µm thick ZnO-based and 8 µm thick $TiO_2$-based DSCs.

## 4. Conclusions

Through a simple and low cost two-step method, based on RF magnetron sputtering deposition and thermal oxidation, a sponge-like ZnO nanostructured films with thicknesses up to 18 µm were obtained. They present a high density of branches, a relatively high specific area value, fine optical transmittance and a suitable dye loading amount.

DSC photoanodes were fabricated using the sponge-like ZnO nanostructures. These photoanodes exhibit enhanced transport properties if compared to the $TiO_2$ nanoparticle-based ones. Open circuit voltage decay measurements and electrochemical impedance spectroscopy modelling evidence high charge lifetime and diffusion coefficient values for the ZnO based cells. A reduced recombination rate and an increased diffusion length with respect to a standard $TiO_2$ nanoparticle-based DSC were achieved thanks to a more direct pathway for the electron collection.

The fabricated DSCs were characterized in terms of photovoltaic performance: the noticeable photoconversion efficiency value of 6.67% was obtained using an 18 µm thick ZnO layer.

In addition, thanks to the relatively low oxidation temperature it will be possible, in the future, to fabricate flexible photoanode exploiting the same ZnO nanostructures and high-temperature resistant polymeric substrate (for example polyimide).

## Acknowledgements

Authors would like to thank Dr. M. Armandi for the fruitful discussions.

## Notes and references

[a] *Center for Space Human Robotics @PoliTo, Istituto Italiano di Tecnologia, Corso Trento 21, 10129, Turin, Italy. Fax: +39 011 5643401; Tel: +39 011 0903413; E-mail: adriano.sacco@iit.it*
[b] *Applied Science and Technology Department, Politecnico di Torino, Corso Duca degli Abruzzi 24, 10129, Turin, Italy.*
[c] *Department of Electronics and Telecommunications, Politecnico di Torino, Corso Duca degli Abruzzi 24, 10129, Turin, Italy.*

1 B. O'Regan and M. Grätzel, *Nature*, 1991, **353**, 737.
2 A. Yella, H. W. Lee, H. N. Tsao, C. Yi, A. K. Chandiran, M. K. Nazeeruddin, E. W. G. Diau, C. Y. Yeh, S. M. Zakeeruddin and M. Grätzel, *Science*, 2011, **334**, 629.
3 C. Bauer, G. Boschloo, E. Mukhtar and A. Hagfeldt, *J. Phys. Chem. B*, 2001, **105**, 5585.
4 A. B. F. Martinson, J. E. McGarrah, M. O. K. Parpia and J. T. Hupp, *Phys. Chem. Chem. Phys.*, 2006, **8**, 4655.
5 M. Law, L. E. Greene, J. C. Johnson, R. Saykally and P. Yang, *Nat. Mater.*, 2005, **4**, 455.
6 T. Zhang, W. Dong, M. Keeter-Brewer, S. Konar, R. N. Njabon and Z. R. Tian, *J. Am. Chem. Soc.*, 2006, **128**, 10960.
7 H. M. Cheng, W. H. Chiu, C. H. Lee, S. Y. Tsai and W. F. Hsieh, *J. Phys. Chem. C*, 2008, **112**, 16359.
8 J. B. Baxter and E. S. Aydil, *Sol. Energ. Mat. Sol. C.*, 2006, **90**, 607.
9 C. Cheng, Y. Shi, C. Zhu, W. Li, L. Wang, K. K. Fung and N.Wang, *Phys. Chem. Chem. Phys.*, 2011, **13**, 10631.
10 I. Gonzalez-Valls and M. Lira-Cantu, *Energ. Environ. Sci.*, 2009, **2**, 19.
11 K. Keis, E. Magnusson, H. Lindström, S. E. Lindquist and A. Hagfeldt, *Sol. Energ. Mat. Sol. C.*, 2002, **73**, 51.
12 N. Memarian, I. Concina, A. Braga, S. M. Rozati, A. Vomiero and G. Sberveglieri, *Angew. Chem.-Int. Edit.*, 2011, **50**, 1.
13 R. Gazia, A. Chiodoni, S. Bianco, A. Lamberti, M. Quaglio, A. Sacco, E. Tresso, P. Mandracci and C. F. Pirri, *submitted*.
14 A. Lamberti, R. Gazia, A. Sacco, S. Bianco, M. Quaglio, A. Chiodoni, E. Tresso and C. F. Pirri, *Prog. Photovolt: Res. Appl.*, 2012, *in press,* DOI: 10.1002/pip.2251.
15 A. Lamberti, A. Sacco, S. Bianco, E. Giuri, M. Quaglio, A. Chiodoni and E. Tresso, *Microelectron. Eng.*, 2011, **88**, 2308.
16 A. Sacco, A. Lamberti, M. Quaglio, S. Bianco, E. Tresso, A.-L. Alexe-Ionescu and C. F. Pirri, *Int. J. Photoenergy*, 2012, **2012**, art. no. 216780.
17 K.-J. Hwang, S.-J. Yoo, S.-H. Jung, D.-W. Park, S.-I. Kim and J.-W. Lee, *Bull. Korean Chem. Soc.*, 2009, **30**, 172.
18 W. Chen, Y. Qiu and S. Yang, *Phys. Chem. Chem. Phys.*, 2010, **12**, 9494.
19 T. Stergiopoulos, A. Ghicov, V. Likodimos, D. S. Tsoukleris, J. Kunze, P. Schmuki and P Falaras, *Nanotechnology*, 2008, **19**, 235602.
20 H.-J. Koo, Y. J. Kim, Y. H. Lee, W. I. Lee, K. Kim and N.-G. Park, *Adv. Mater.*, 2008, **20**, 195.
21 K. Keis, J. Lindgren, S. E. Lindquist and A. Hagfeldt, *Langmuir*, 2000, **16**, 4688.
22 A. Zaban, M. Greenshtein and J. Bisquert, *ChemPhysChem*, 2003, **4**, 859.
23 H. Wang, M. Liu, M. Zhang, P. Wang, H. Miura, Y. Cheng and J. Bell, *Phys. Chem. Phys. Chem.*, 2011, **13**, 17359.
24 J. Halme, P. Vahermaa, K. Miettunen and P. Lund, *Adv. Mater.*, 2010, **22**, E210.
25 J. Bisquert, G. Garcia-Belmonte, F. Fabregat-Santiago, N.S. Ferriols, P. Bogdanoff and E.C. Pereira, *J. Phys. Chem. B,* 2000, **104**, 2287.
26 J. Bisquert and V. S. Vikhrenko, *J. Phys. Chem. B*, 2004, **108**, 2313.
27 H. Wang, M. Liu, C. Yan and J. Bell, *Beilstein J. Nanotechnol.*, 2012, **3**, 378.
28 M. Law, L. E. Greene, J. C. Johnson, R. Saykally and P. Yang, *Nat. Mater.*, 2005, **4**, 455.
29 A. B. F. Martinson, M. S. Góes, F. Fabregat-Santiago, J. Bisquert, M. J. Pellin and J. T. Hupp, *J. Phys. Chem. A*, 2009, **113**, 4015.
30 C. Cheng, Y. Shi, C. Zhu, W. Li, L. Wang, K. K. Fung and N. Wang, *Phys. Chem. Chem. Phys.*, 2011, **13**, 10631.